The effect of number of layers of nanoporous gold films on their electrochemical behaviour

Shan, Zhengyang; Jansen, Charlotte Uldahl; Yesibolati, Murat Nulati; Yan, Xiaomei; Qvortrup, Katrine; Ulstrup, Jens; Xiao, Xinxin

Published in:
Electrochimica Acta

Link to article, DOI:
10.1016/j.electacta.2024.144233

Publication date:
2024

Document Version
Publisher's PDF, also known as Version of record

Electrochimica Acta 489 (2024) 144233

Contents lists available at ScienceDirect

Electrochimica Acta

journal homepage: www.journals.elsevier.com/electrochimica-acta

The effect of number of layers of nanoporous gold films on their electrochemical behaviour

Zhengyang Shan [a], Charlotte Uldahl Jansen [a], Murat Nulati Yesibolati [b], Xiaomei Yan [c], Katrine Qvortrup [a,*], Jens Ulstrup [a,*], Xinxin Xiao [d,*]

[a] Department of Chemistry, Technical University of Denmark, 2800, Kongens Lyngby, Denmark
[b] DTU Nanolab - National Center for Nanofabrication and Characterization, Technical University of Denmark, 2800, Kongens Lyngby, Denmark
[c] Lanzhou Institute of Chemical Physics, Chinese Academy of Science, Lanzhou, 730000, China
[d] Department of Chemistry and Bioscience, Aalborg University, 9220, Aalborg, Denmark

ARTICLE INFO

Keywords:
Nanoporous gold
Ferrocenemethanol
Dopamine
Fructose dehydrogenase
Electrochemistry

ABSTRACT

Nanostructured material based electrodes are frequently used in electrochemical analysis and catalysis for their multifarious favourable properties. The deep interior surfaces of these electrodes are, however, not often well addressed due to diffusion constrains, leading to a poor materials economy. The present work demonstrates thickness control and manipulation of dealloyed nanoporous gold (NPG) electrodes using a layer-by-layer method. The viability of the method is confirmed by electron microscopy and electrochemical characterisation. The effect of the number of NPG layers (from one to five, leading to a thicknesses range of 100–500 nm) on the electrochemical behaviour is evaluated, based on the 1) redox behaviour of a diffusing redox probe ferrocenemethanol, 2) dopamine undergoing proton-coupled two-electron transfer, 3) surface-confined osmium complex modified redox polymer, and 4) the bioelectrocatalysis of an enzyme, fructose dehydrogenase (FDH). Notably, the results show that the best performance is achieved for an intermediate number of NPG layers, suggesting that the tedious efforts in fabricating deep/ thick nanostructures can be optimised.

1. Introduction

Use of nanomaterial modifiers on electrode substrates including carbon and gold based electrode materials is a well-adopted strategy to improve the performance of electrochemical analysis and catalysis [1–4]. Amongst such materials, porous electrodes constitute a major group of high-specific-surface-area electrodes [5,6], which can be fabricated by template or non-template methods. They can be used either directly as functional surfaces, such as in the detection of the neurotransmitter dopamine with electrochemical surface redox processes [7], or as a support surface modified with functional selective catalysts, such as for immobilized oxidoreductase enzyme bioelectrodes [2,8]. For the former case, the effective surface area of the porous electrode is crucial, while the catalyst carrying ability is what matters for the latter case.

The surface geometry of a porous electrode, especially the pore diameter plays a crucial role in the resulting electrochemical behaviour. In a typical so-called dealloying process, gold alloyed with other, less noble metals (such as Ag, Zn, Cu) are used as precursors, which are chemically or electrochemically etched. The less noble metals are selectively etched. The remaining gold atoms undergo surface diffusion, and aggregate into clusters and islands rather than spreading over the surface. This process results in dealloyed nanoporous gold (NPG) in porous structures with tuneable pore sizes [9–12]. The pore size (diameter) exhibits an inversely proportional relationship to the real (electrochemically active) surface. The latter is typically obtained via surface controlled oxidation of gold atoms at the outermost surface area [6]). Small pore size is typically preferred given the large surface area. This is consistent for example with the report by Chen and associates showing that the highest catalytic response to the electro-reduction of hydrogen peroxide on a series of variable-diameter NPG electrodes was obtained at NPG of 18 nm pores with the largest effective working area, over those of 30, 40 and 50 nm diameter [13]. It is, however, noteworthy that intermediate pore diameters typically offer the best performance for bioelectrochemical studies when large size enzyme molecules are immobilized. This could for example explain, why Chen and associates found that the best response to glucose oxidase (GOx) catalysed electro-oxidation of glucose was obtained for NPG of 30 nm,

* Corresponding authors.
E-mail addresses: kaqvo@kemi.dtu.dk (K. Qvortrup), ju@kemi.dtu.dk (J. Ulstrup), xixi@bio.aau.dk (X. Xiao).

https://doi.org/10.1016/j.electacta.2024.144233
Received 18 December 2023; Received in revised form 6 February 2024; Accepted 6 April 2024
Available online 6 April 2024

over diameters of 18, 40 and 50 nm [13]. Biomolecules cannot effectively enter the inner pores especially when the pore size is smaller than the size of the molecules themselves (including water hydration shells). Such a pore size effect on bioeletrochemical behaviour has been found, for example, for cytochrome *c* on NPG [11], and for bilirubin oxidase (BOx) on NPG [14], fructose dehydrogenase (FDH) on NPG [15], and BOx on porous carbon [16].

The depth of the nanostructured region of an electrode or the thickness of the nanoporous film is another important factor in the design of porous electrodes. Previous results for the direct electrooxidation of glucose on porous platinum electrodes, however, imply that the tedious efforts in fabricating a very deep/ thick nanostructure may not always be needed [17], as the deeper pore structure is not electrochemically addressed. This is especially the case in enzymatic bioelectrochemistry, as enzyme substrate mass transfer is often the limiting factor. The simulation of a H_2-air enzymatic biofuel cell (EBFC) using a three-dimensional porous electrode thus showed that bioelectrodes thicker than 250 μm cannot further enhance the current density of the EBFC [18]. On the other hand, Siepenkoetter and associates found that higher current density towards the BOx catalysed dioxygen reduction reaction was achieved on 500-nm-thick NPG films over those on 100- and 300-nm NPG [14]. Also, NPG films dealloyed from substrate-supported Au-Ag alloy undergo stress release on volume contraction, leading to cracks (typically with a length in a range of 200–4000 nm, which is considerably larger that the pore size) on the NPG. The cracks were found to be larger on thicker NPG films [14]. Crack-free NPG films with different thicknesses are thus needed for meaningful comparison. NPG films obtained from etching free-standing Au-Ag leaves are free of cracks [6,9,19].

In order to illuminate the core issue of the importance of the thickness, or depth of nanostructured porous electrodes, we report here a systematic study of the NPG thickness using a feasible NPG preparation method that ascertains crack-free NPG preparation. Our preparation rests on a simple layer-by-layer approach to stack free-standing NPG films to form a multilayer electrode (Scheme 1). This approach allows stacking of relatively thin NPG films (≅ 100 nm or so) thus minimizing the risk of crack formation. The electrodes were characterized by a variety of structural and electrochemical methods that testify towards the crack-free nature of the electrode material. The electrochemical behaviour of the electrodes was probed using different representative target redox processes i.e.: NPG surface activation in sulfuric acid; diffusion-controlled ferrocene-methanol (FcOH) voltammetry; surface-sensitive dopamine monolayer voltammetry; and voltammetry of surface-bound osmium-complex modified redox polymer. Enzymatic bioelectrochemical behaviour, i.e., the direct electron transfer (DET) of FDH, on multilayer NPG was also studied. Notably, the optimal performance was overall achieved for an intermediate number of NPG layers.

2. Experimental section

2.1. Chemicals and materials

FDH from *Gluconobacter* sp. (EC 1.1.99.11, activity: 80 U mg^{-1}) was from Sorachim Chemicals, Switzerland. Sulfuric acid (H_2SO_4, 95–97 %), ferrocene-methanol (FcOH, 97 %), 2-mercaptoethanol ($HS(CH_2)_2OH$, BME, ≥ 99.0 %), dopamine hydrochloride (DA), fructose (≥ 99.0 %), disodium hydrogen phosphate dodecahydrate ($Na_2HPO_4{\cdot}12H_2O$, ≥ 99.0 %), sodium phosphate monobasic monohydrate ($NaH_2PO_4{\cdot}H_2O$, ≥ 99.5 %), and 3,4-ethylenedioxythiophene (EDOT, 97 %) were from Sigma-Aldrich, nitric acid (HNO_3, 70 %) from Fisher Scientific, UK. 0.1 M pH 5.5 McIlvaine buffer solution was prepared by mixing solutions of citric acid and Na_2HPO_4. 0.1 M pH 7.0 phosphate buffer solution (PBS) was prepared by mixing solutions of Na_2HPO_4 and NaH_2PO_4 with the proper ratio. All chemicals were used without any purification, and all solutions were prepared with Milli-Q water (18.2 MΩ cm). $[Os(2,2'\text{-bipyridine})_2(\text{polyvinylimidazole})_{10}Cl]^{+/2+}$ ($Os(bpy)_2PVI$) was a gift from Prof. Dónal Leech at the University of Galway.

2.2. Preparation of stacked multiple-layer npg films

NPG leaves were fabricated by dealloying ca. 100 nm thick Au/Ag alloy leaves (12-carat, Eytzinger, Germany) in concentrated HNO_3 for 30 min at 30 °C, Scheme 1. This resulted in NPG films with an average pore size of ca. 30 nm [9,19]. The NPG films were then attached onto pre-polished glassy carbon electrodes (GCEs) with a diameter of 4 mm. When the first NPG film was dry and modified by removing the excess part covering the GCE, the second NPG film was attached. The electrodes with multilayer of NPG films were prepared by successive application of the same process. Up to five layers of NPG films can be obtained in such a "layer-by-layer" approach. Prior to use, cyclic voltammetry (CV) of NPG in 1 M H_2SO_4 was carried out to create clean surfaces and left to dry naturally. 15 rounds of CVs were scanned, as it was found that the voltammograms had stabilized over at least 15 cycles [9,20].

2.3. FDH immobilization on npg electrodes

Following our previously published protocol [8,21], a self-assembled monolayer of BME on the NPG electrodes was first prepared by soaking the NPG electrodes in 3 mM BME solution for 24 h. NPG-BME electrodes

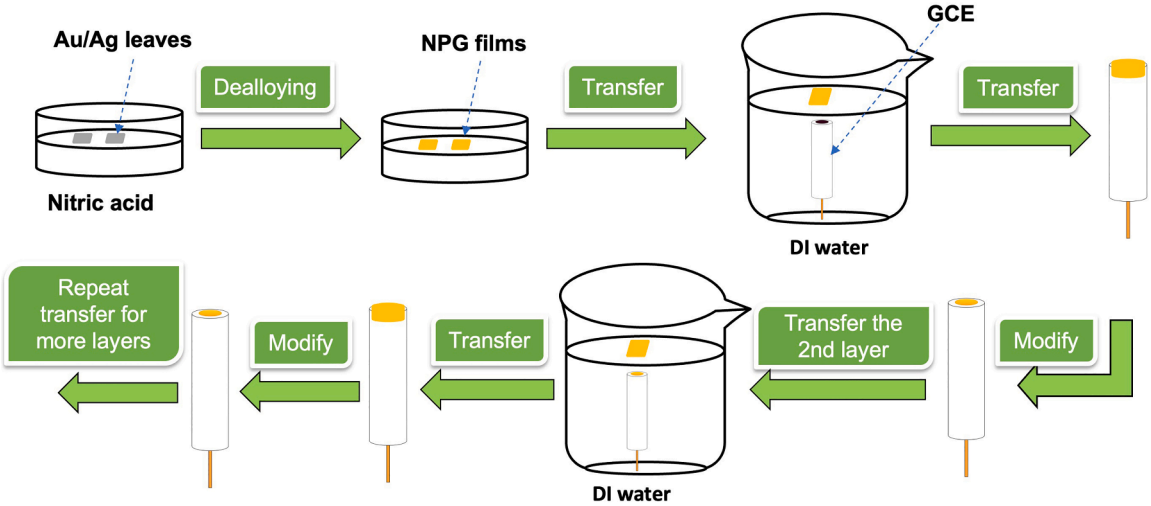

Scheme 1. The procedure used to prepare stacked multilayers of NPG films.

were then immersed into 0.6 g/L FDH solution for another 24 h at 4 °C, leading to the noncovalent binding of enzyme onto the electrode.

2.4. Scanning electron microscopy (SEM)

NPG in various stacking layers were prepared on a normal copper tape. The morphology and microstructure, as well as the cross-section profiling, of NPG were characterized by field emission scanning electron microscopy (FE-SEM, Quanta FEG 200, USA) with an acceleration voltage of 20 kV.

2.5. Electrochemical characterization

Electrochemical characterization was conducted using an Autolab instrument (PGSTAT12, Eco Chemie, Netherlands) or a PalmSens 3 potentiostat (PalmSens, Netherlands). NPG and modified NPG electrodes were used as the working electrode. A Ag/AgCl in saturated KCl solution was the reference electrode and a platinum electrode the counter electrode. All electrochemical measurements were carried out at ambient temperature (ca. 20 °C).

To test the electrochemical behaviour of NPG in FcOH and DA, 5 mM FcOH or 1 mM DA, freshly prepared to avoid auto-oxidation [22], in Ar-saturated 0.1 M pH 7.0 PBS, respectively was used as electrolyte. CVs at a range of scan rates were recorded.

PEDOT/Os(bpy)$_2$PVI was electrodeposited in 0.1 M pH 7.0 PBS containing 2 mM polyethylene glycol 3400, 20 mM EDOT, and 0.5 mg ml^{-1} Os(bpy)$_2$PVI, with a 300 s pulse sequence of 0.9 V (2 s) and −0.4 V (3 s) [23].

To test the electrocatalytic performance of FDH modified NPG [21], both direct electron transfer (DET) and mediated electron transfer (MET) processes were studied. For DET, Ar-saturated 0.1 M pH 5.5 McIlvaine buffer [21] with and without 100 mM fructose was used. 0.1 M pH 5.5 McIlvaine buffer containing 0.5 mM FcOH with and without 100 mM fructose was adapted for MET with FcOH as ET mediator.

3. Results and discussion

3.1. Morphology of the multilayer npg electrodes

The microstructure of the as-prepared NPG films was characterised by SEM, Fig. 1. Observed from top view, NPG shows a bi-continuous porous structure with randomly distributed pores and 30 nm average pore size (Fig. 1A). Cross-sections of the multilayer NPG films exhibit distinct boundaries between the layers (Fig. 1B-E). Each layer is about 100 nm thick. The average thicknesses of different samples were determined to be 187±6 (2-layer), 338±7 (3-layer), 377±9 (4-layer) and 518±6 nm (5-layer), respectively. Multiple layers are closely stacked with each other, with no indications of cracks in the films. The seen gaps in Fig. 1E most likely come from the sample preparation for SEM. To see the cross-section profile by SEM, NPG films were stacked on a copper tape and manually cut by scissors. The gap between each film is also anticipated to be extremely small during electrochemical testing. Otherwise, the NPG film will be broken during the electrochemical activation in H_2SO_4. SEM cannot provide information about the

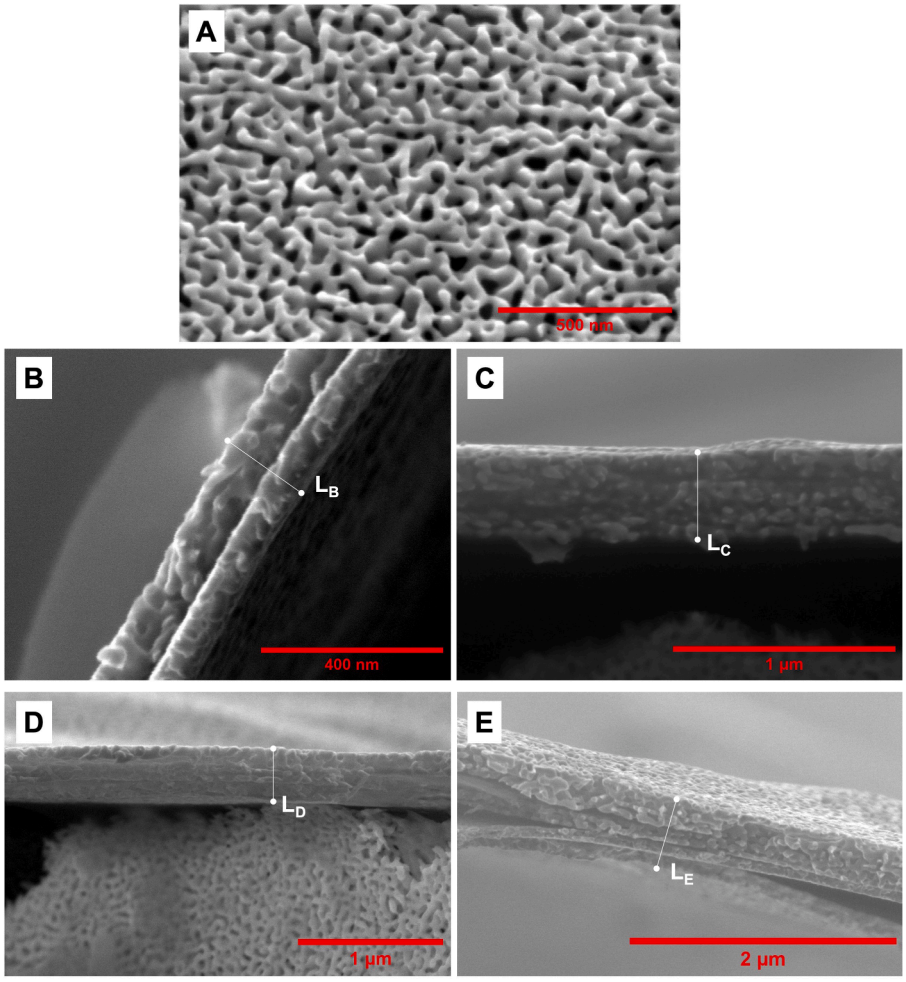

Fig. 1. SEM images of the NPG films in top-down view (A), and cross-section profiles in two (B), three (C), four (D) and five (E) layers. L refers to the thickness of the corresponding film.

alignment of the randomly distributed pores which, however, cannot be well controlled by the present layer-by-layer approach.

3.2. Electrochemical activation of the multilayer npg electrodes

CV of NPG in 1 M H_2SO_4 is an established procedure for gold-based electrodes, denoted as "electrochemical activation", as residual silver atoms on the surface can be removed and a clean gold surface created in a surface controlled redox process [10]. The outermost gold atoms undergo oxidation at potentials higher than 1.1 V, showing fingerprint oxidation peaks corresponding to the Au (100), Au (110) and Au (111) facets, Fig. 2A [6,9,19]. The sharp reductive peak corresponding to the reduction of gold oxide can be integrated and the total charge associated with the real, electrochemically active surface area determined [6]. A constant, the specific charge of 390 μC cm^{-2} for gold oxide reduction [24], is widely-accepted to calculate the NPG roughness factor, i.e., the ratio of the real to the geometric surface area [6].

Fig. 2A shows that the reduction peak increases with increasing number of NPG layers. The calculated roughness factor displays a linear correlation to the number of NPG layers, with a slope of 6.7 ± 0.2 per layer, a value that matches well the roughness of a single NPG layer (8.7 ± 1.3) Fig. 2B. The results confirm that almost all the NPG surface, up to 5 layers of ca. 500 nm, can be soaked by 1 M sulfuric acid and electrochemically addressed.

3.3. Electrochemistry of redox active molecules on the multilayer npg electrodes

Voltammetry of several types of redox molecules on the NPG electrodes was recorded. FcOH is commonly used both as redox probe and as mediator for bioelectrodes [8,21], undergoing a typical diffusion controlled redox process and thus not very sensitive to the particular electrode surface. Dopamine is an important neurotransmitter and an intriguing electroanalytical target. The redox behaviour of dopamine is sensitive to the electrode surface [25]. Comparison of the CVs of NPG electrodes between FcOH and dopamine is therefore of importance. We further investigated CVs of a surface-bound osmium-complex modified redox polymer, which is a versatile platform for both electrochemical enzyme immobilization and ET mediation [23,26-29].

CVs of 5 mM FcOH at different scan rates are shown in Fig. 3A-E. A pair of well-defined, close to reversible oxidation and reduction peaks is displayed. Both peak heights increase with increasing scan rate, exhibiting a perfect linear relationship between the peak intensity and square root of the scan rate, indicative of a diffusion-controlled redox process. This pattern is apparent for all the electrodes (1- to 5-layer). The CVs at the low scan rate of 5 mV s^{-1} displays no enhancement with increasing number of NPG layers (Fig. 3F), confirming the independence of the redox behaviour of FcOH on the surface roughness. This is because the redox process of FcOH is fast, validated from the narrow peak separations (ca. 73 mV at 5 mV s^{-1}) of the oxidation and reduction peaks, accomplished when only the outermost regions of the NPG pores are operative [9,12]. This may also explain why the peak intensities are slightly enhanced by increasing the number of NPG layers at the high scan rate of 500 mV s^{-1} (Fig. 3G).

CV of 1 mM dopamine is shown in Fig. 4A-E. Dopamine undergoes a classical ECE mechanism, where E and C refer to the electrochemical and chemical steps, respectively [30,31]. The proton-coupled [32] two-electron oxidation product of dopamine is dopaminoquinone (DOQ) [25,33]. The redox conversion between dopamine and DOQ occurs between 0.2 and 0.3 V vs. Ag/AgCl. DOQ is chemically converted into leucodopaminechrome (LC) via a 1,4-Michael addition [34]. The proton-coupled two-electron redox reaction between LC and dopaminechrome (DC) occurs at ca. −0.2 V vs. Ag/AgCl, with both smaller current densities and smaller peak separations in comparison to those of dopamine/ DOQ. Both redox reactions are electrochemically reversible.

The electrochemical detection of dopamine often rests on the dopamine/ DOQ conversion, likely due to its higher current responses than those of LC/ DC [25]. The same voltammetric pattern as for FcOH is otherwise observed for dopamine, i.e. the absolute values of the redox peaks increase with increasing scan rate. Unlike that of FcOH, the current densities of the redox peaks are found to be proportional to the 0.62th power of the scan rate (**Figure S1**). The value between 0.5 and 1 is indicative of a mixed diffusion and surface controlled redox process [35,36]. This is further confirmed by the observation that the redox peaks are enhanced by increasing the number of NPG layers at both low and high scan rates (Fig. 4F-G). Notably the enhancement is not as high as the increase of the number of the NPG layers (for example only 1.5 fold for 1–3-layers at 600 mV s^{-1}, Fig. 4F). It is also clear that enhancement is no longer obvious when the number of layers is larger than three. Altogether this implies that a moderate depth profile of the nanostructure is sufficient for optimized electrochemical sensing of dopamine. Additional efforts to prepare thicker nanostructures can thus be spared, which is highly beneficial from the point view of economy of materials fabrication.

Electrodeposited composite polymer of PEDOT/$Os(bpy)_2$PVI [23] is another redox probe on NPG electrodes that we have investigated. Osmium complexes are robust molecular entities as ET mediators, and also core electrochemical probes due to insignificant structural reorganization and therefore fast, close to reversible "kinetically unhindered" interfacial ET processes [37]. As the redox polymer is now bound to the electrode surface, the redox behaviour is surface controlled, suggesting a linear relationship between peak current and scan rate. In fact, diffusion

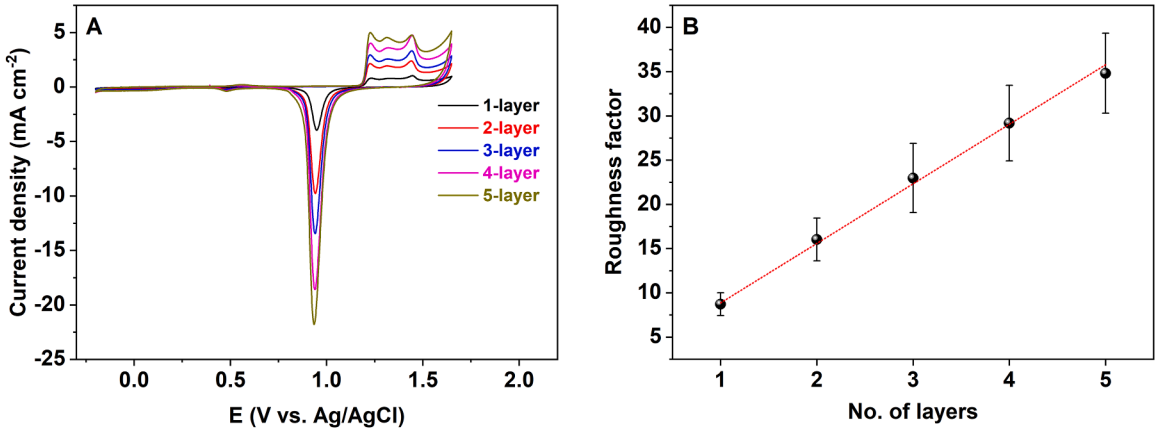

Fig. 2. (A) Cyclic voltammograms (CVs) of variable-thickness NPG film electrodes in Ar-saturated 1 M H_2SO_4; scan rate 100 mV s^{-1}. (B) Corresponding roughness factors based on integration of the reduction peak of the gold oxide formed.

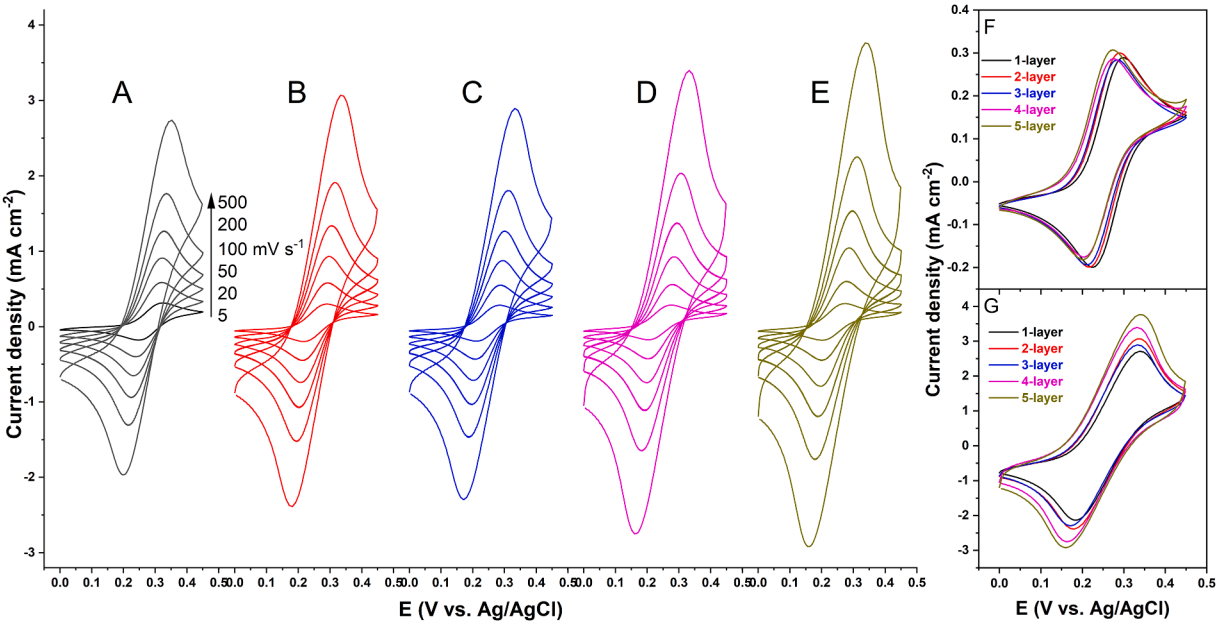

Fig. 3. CVs of variable-layer NPG film electrodes (A: one layer; B: two layers; C: three layers; D: four layers; E: five layers) in 5 mM FcOH in Ar-saturated 0.1 M pH 7.0 PBS. Overlays of CVs at 5 (F) and 500 (G) mV s^{-1}.

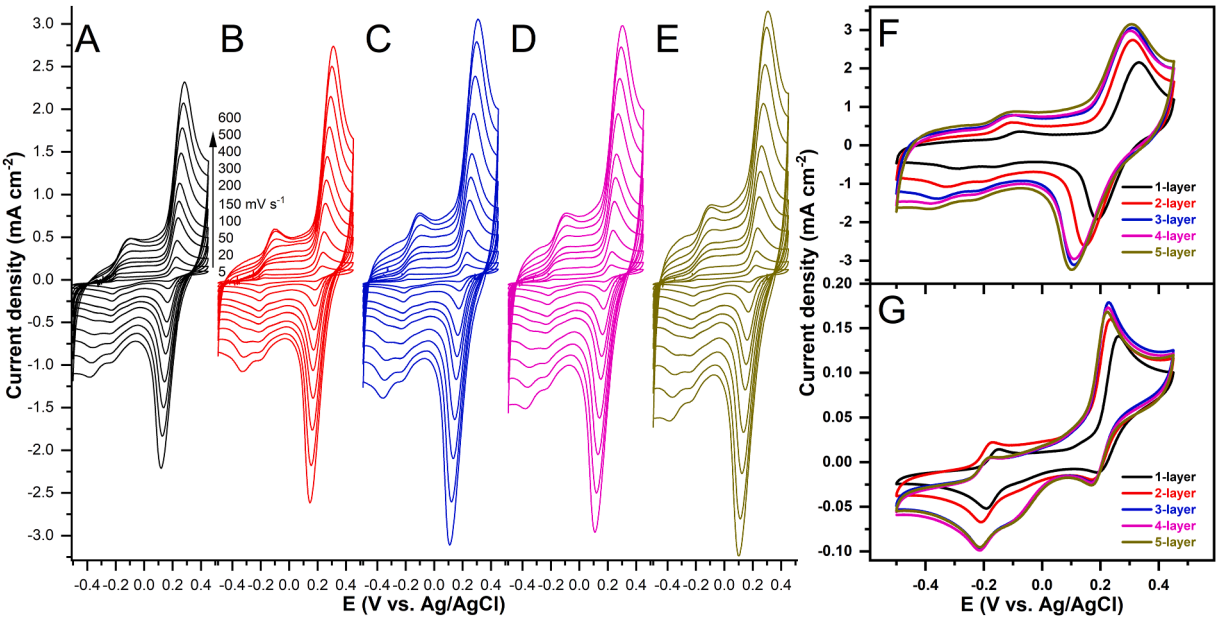

Fig. 4. CVs of variable-thickness NPG film electrodes (A: one layer; B: two layers; C: three layers; D: four layers; E: five layers) in 1 mM DA in Ar-saturated 0.1 M pH 7.0 PBS. Overlays of CVs at 600 (F) and 5 (G) mV s^{-1}.

also appears involved as the redox film has a certain thickness especially when swelling in the solution, and the electrons have to "diffuse", or "hop" along the Os(II)/(III) centres across the film to the electrode surface [28,32,38]. Both non-faradaic capacitance currents and faradaic currents of the single-electron transfer processes of the osmium complexes are enhanced by the number of the NPG layers, which saturates at four layers (Fig. 5A). After subtracting the background current, the apparent highest surface coverage of electroactive Os species is achieved at three layers (Fig. 5A), suggesting that the inner NPG pore regions are not accessible during the electrodeposition.

3.4. Enzymatic bioelectrochemistry of the multilayer npg electrodes

Enzymatic bioelectrochemistry of *Gluconobacter* sp. FDH is a final variable-layer NPG target of ours. This enzyme is a fructose oxidising, membrane-bound DET capable and redox active enzyme [39], with applications in biofuel cells and biosensors. FDH is a heterotrimeric flavohemoprotein. Subunit I of FDH contains a covalently bound FAD, where the two-electron oxidation of fructose occurs. Subunit II has three haems with various redox potentials that transmit the electrons from the subunit I. Ubiquinone-10 (UQ_{10}) is weakly bound to FDH, playing a role in the intramolecular ET to ubiquinol oxidase [40]. A small subunit III accounts for structural integrity, and is not involved in the ET pathway. Very recently, cryo-electron microscopy has disclosed the presence of a

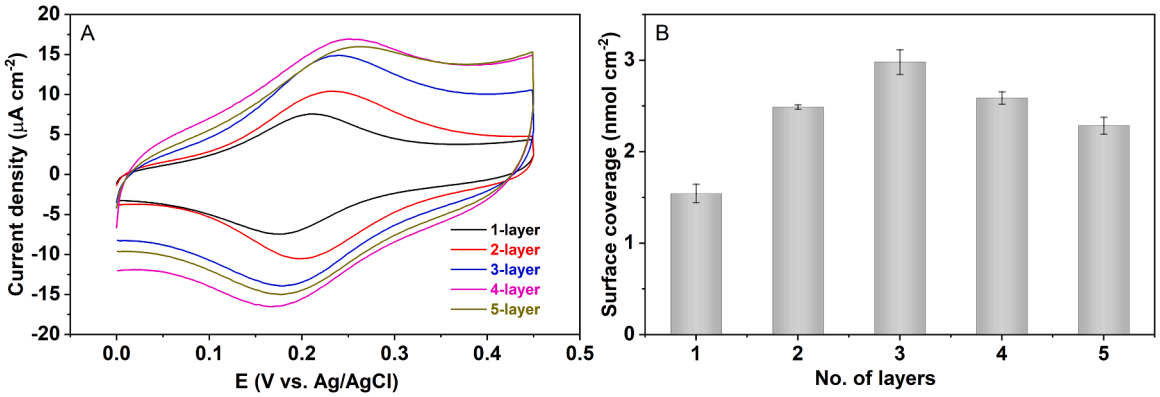

Fig. 5. (A) CVs of variable-thickness NPG/PEDOT/Os(bpy)$_2$PVI in Ar-saturated 0.1 M pH 7.0 PBS at 5 mV s^{-1}. (B) The calculated surface coverage of electroactive Os-centre of the Os polymer on the electrode.

3Fe-4S iron-sulfur cluster (3Fe4S, $E^0 = -0.130$ V vs. Ag/AgCl), serving as an additional ET relay between FAD ($E^0 = -0.267$ V vs. Ag/AgCl) and haem 3c ($E^0 = -0.011$ V vs. Ag/AgCl) [40]. Due to the long distance from haem 2c ($E^0 = +0.065$ V vs. Ag/AgCl) and high E^0 of UQ_{10} and haem 1c, these centres are not directly engaged in the DET towards the electrode surface, although they are involved in the natural biological ET to ubiquinol oxidase. Instead, haem 2c is widely accepted to be the ET outlet to the electrode surface (Scheme 2).

2-mercaptoethanol (BME) SAMs on the surface to immobilize FDH on NPG were first prepared, as the BME hydroxyl terminal group was previously found to promote FDH in a DET-capable orientation [21]. FDH is then adsorbed onto the NPG-SAM electrodes, with a reasonable storage stability. The FDH at 4-layer NPG retains 30 % of its DET activity in the time course of 10 days' storage at 4 °C (**Figure S2**). As shown in Fig. 6A-E, DET profiles towards 100 mM fructose show an onset potential of ca. −0.05 V vs. Ag/AgCl, slightly lower than that of haem 2c ($E^0 = +0.065$ V vs. Ag/AgCl). FcOH further introduced here as a diffusing mediator (Fig. 6F-J), leads to mediated ET (MET) between FDH and NPG. The MET current density reflects the total active amount of surface confined FDH enzymes [21,41], irrespective of their orientation suitable for DET. Multi-layer NPG gives higher MET signal than that of the single layer, indicative of a greater enzyme carrying capacity, attributed to the increased electrode roughness factor. Regarding the effect of the number of NPG layers, the DET current density of four-layer NPG gives the highest current density (Fig. 6D and Fig. 7), consistent with the largest MET current density (Fig. 6I and Fig. 7). Five-layer NPG does not register a higher response, most likely because the inner layers are not addressable by the large biomolecule. The results here again indicate that efforts towards preparing thicker and more complex nanostructures do not necessarily pay off, since a compromise thickness is the best choice.

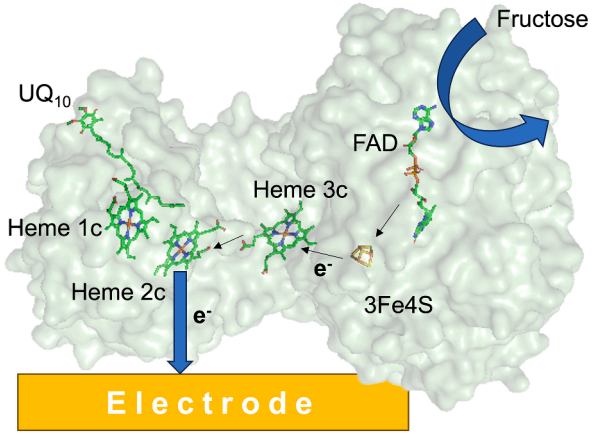

Scheme 2. Schematic drawing of the DET mechanism of FDH (PDB: 8JEJ [40]) at an electrode surface.

4. Conclusions

We have introduced a highly convenient layer-by-layer approach to prepare a variety of multilayer NPG film electrodes. The properties of the new films are validated by SEM and multifarious electrochemical characterization. Particularly, SEM disclosed no structural "cracks" in the new multilayer NPG structures. The NPG multilayers attached to the GCE were also found to be closely attached to each other in SEM, and reasonably considered not to affect the electrochemical tests. The surface oxidation of gold allows determining the roughness factor, which is the numerical descriptor of the real, electrochemically active surface area. Importantly, this area was found to be proportional to the number of NPG layers.

The NPG electrodes were studied in detail for their electrochemical behaviour, first by straightforward diffusion controlled FcOH voltammetry, then by mixed diffusion and surface controlled redox behaviour of dopamine and surface-bound Os polymer, and finally by the complex enzyme FDH voltammetry. Increasing the number of NPG layers shows no enhancement of the FcOH redox waves at low scan rates, but slight enhancement at high scan rates, indicative that variable electrode surface areas are operative at different NPG electrode thickness. The enhancement factor is thus not as profound as the roughness factor. The same applies to the current signals of our other primary target systems, dopamine, Os polymer, and FDH. A major new result of ours is that we found that typically three or four layers of our novel variable-layer NPG electrode materials, corresponding to 300–400 nm thickness, contribute the best performance for all the multifarious selected systems. Overarchingly, these results can be ascribed to a compromise between increased surface area and constrained diffusion.

Our multi-layer NPG electrode materials therefore offer new electrochemical materials science based on controlled preparation of variable-thickness defect-free ("crack-free") NPG. The electrochemical properties of the new NPG materials can furthermore be optimized by systematic variation of the NPG layer numbers and overall thickness of the NPG electrode materials. Future projects would suggest fabricating new configurations of multilayered NPG, such as a hierarchical structure with the inner NPG structure of larger pore size and outer NPG structure with smaller pore size, so that diffusion constraints can be alleviated. Regarding practical application, robust NPG films obtained from substrate supported precursors can be fabricated in a large and massive scale.

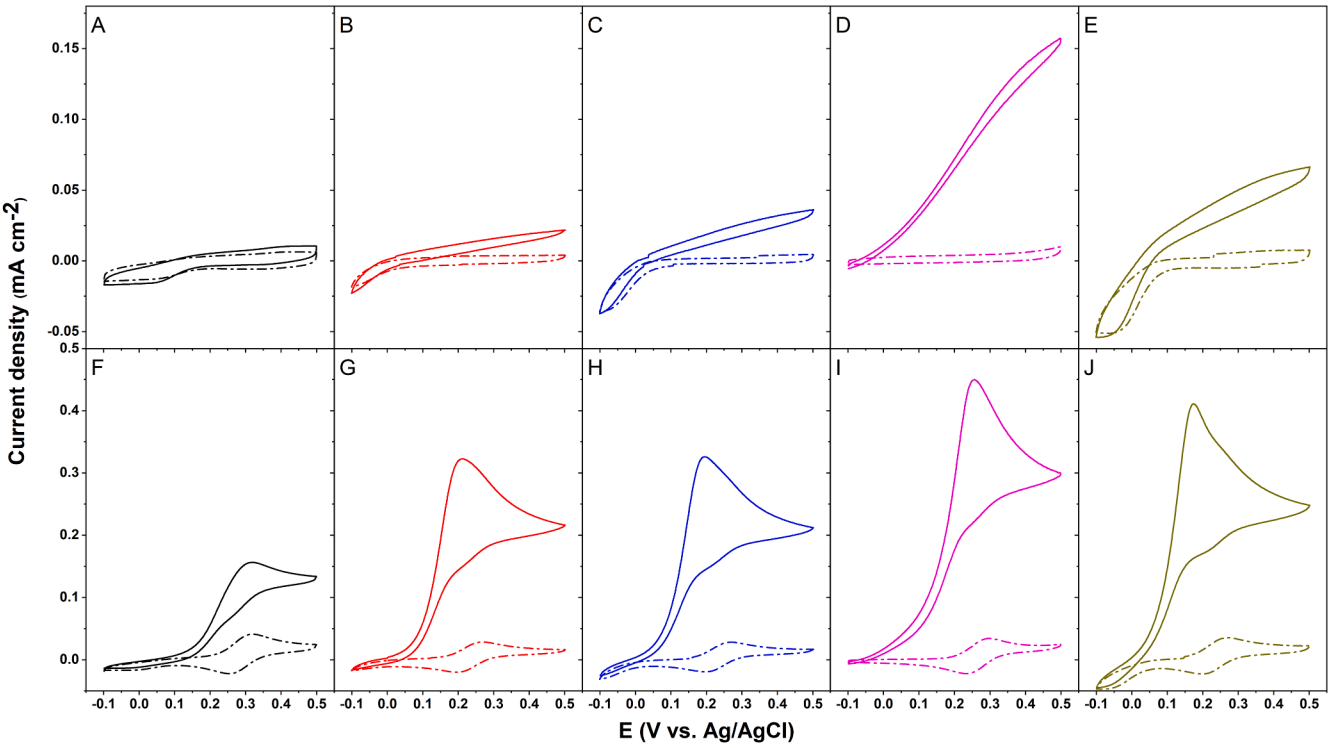

Fig. 6. CVs of variable-layer NPG film electrodes with adsorbed FDH. (A, F: one layer; B, G: two layers; C, H: three layers; D, I: four layers; E, J: five layers). Ar-saturated 0.1 M pH 5.5 McIlvaine buffer in the absence (dash-dotted line) and presence (solid line) of 100 mM fructose undergoing either DET (A-E) or MET (F-J) using 0.5 mM FcOH as the mediator.

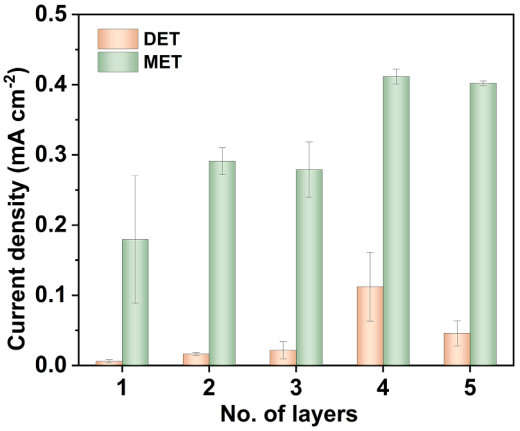

Fig. 7. Dependence of DET and MET current densities on the number of layers of NPG films. Data summarized from Fig. 5.

CRediT authorship contribution statement

Zhengyang Shan: Visualization, Investigation, Data curation. **Charlotte Uldahl Jansen:** Writing – review & editing, Supervision, Data curation. **Murat Nulati Yesibolati:** Data curation. **Xiaomei Yan:** Data curation. **Katrine Qvortrup:** Writing – review & editing, Supervision. **Jens Ulstrup:** Writing – review & editing, Supervision, Investigation. **Xinxin Xiao:** Writing – review & editing, Writing – original draft, Supervision, Methodology, Data curation.

Declaration of competing interest

The authors declare that they have no known competing financial interests or personal relationships that could have appeared to influence the work reported in this paper.

Data availability

Data will be made available on request.

Acknowledgments

X.X. acknowledges a Villum Experiment (grant No. 35844) and a Novo Nordisk Foundation Start Package grant (0081331).

Supplementary materials

Supplementary material associated with this article can be found, in the online version, at doi:10.1016/j.electacta.2024.144233.

References

[1] N. Mano, Recent advances in high surface area electrodes for bioelectrochemical applications, Curr. Opin. Electrochem. 19 (2020) 8–13.
[2] X. Xiao, H.-q. Xia, R. Wu, L. Bai, L. Yan, E. Magner, S. Cosnier, E. Lojou, Z. Zhu, A. Liu, Tackling the challenges of enzymatic (Bio)Fuel Cells, Chem. Rev. 119 (2019) 9509–9558.
[3] L. Qian, S. Durairaj, S. Prins, A. Chen, Nanomaterial-based electrochemical sensors and biosensors for the detection of pharmaceutical compounds, Biosens. Bioelectron. 175 (2021) 112836.
[4] I. Mazurenko, A. de Poulpiquet, E. Lojou, Recent developments in high surface area bioelectrodes for enzymatic fuel cells, Curr. Opin. Electrochem. 5 (2017) 74–84.
[5] J.L. Olloqui-Sariego, J.J. Calvente, R. Andreu, Immobilizing redox enzymes at mesoporous and nanostructured electrodes, Curr. Opin. Electrochem. 26 (2021) 100658.
[6] X. Xiao, P. Si, E. Magner, An overview of dealloyed nanoporous gold in bioelectrochemistry, Bioelectrochem 109 (2016) 117–126.
[7] Q. Cao, P. Puthongkham, B.J. Venton, Review: new insights into optimizing chemical and 3D surface structures of carbon electrodes for neurotransmitter detection, Anal. Methods 11 (2019) 247–261.

[8] C.U. Jansen, X. Yan, J. Ulstrup, X. Xiao, K. Qvortrup, Structural design of anthraquinone bridges in direct electron transfer of fructose dehydrogenase, Colloids Surf. B: Biointerfaces 220 (2022) 112941.
[9] X. Xiao, J. Ulstrup, H. Li, J. Zhang, P. Si, Nanoporous gold assembly of glucose oxidase for electrochemical biosensing, Electrochim. Acta 130 (2014) 559–567.
[10] X. Xiao, T. Siepenkoetter, P.Ó. Conghaile, D. Leech, E. Magner, Nanoporous gold-based biofuel cells on contact lenses, ACS Appl. Mater. Interfaces 10 (2018) 7107–7116.
[11] T. Siepenkoetter, U. Salaj-Kosla, X. Xiao, S. Belochapkine, E. Magner, Nanoporous gold electrodes with tuneable pore sizes for bioelectrochemical applications, Electroanalysis 28 (2016) 2415–2423.
[12] M.D. Scanlon, U. Salaj-Kosla, S. Belochapkine, D. MacAodha, D. Leech, Y. Ding, E. Magner, Characterization of nanoporous gold electrodes for bioelectrochemical applications, Langmuir 28 (2011) 2251–2261.
[13] L.Y. Chen, T. Fujita, M.W. Chen, Biofunctionalized nanoporous gold for electrochemical biosensors, Electrochim. Acta 67 (2012) 1–5.
[14] T. Siepenkoetter, U. Salaj-Kosla, X. Xiao, P.Ó. Conghaile, M. Pita, R. Ludwig, E. Magner, Immobilization of redox enzymes on nanoporous gold electrodes: applications in biofuel cells, Chempluschem 82 (2017) 553–560.
[15] T. Siepenkoetter, U. Salaj-Kosla, E. Magner, The immobilization of fructose dehydrogenase on nanoporous gold electrodes for the detection of fructose, ChemElectroChem 4 (2017) 905–912.
[16] H. Funabashi, S. Takeuchi, S. Tsujimura, Hierarchical meso/macro-porous carbon fabricated from dual MgO templates for direct electron transfer enzymatic electrodes, Sci. Rep. 7 (2017) 45147.
[17] S. Park, Y.J. Song, J.-H. Han, H. Boo, T.D. Chung, Structural and electrochemical features of 3D nanoporous platinum electrodes, Electrochim. Acta 55 (2010) 2029–2035.
[18] I. Mazurenko, K. Monsalve, P. Infossi, M.-T. Giudici-Orticoni, F. Topin, N. Mano, E. Lojou, Impact of substrate diffusion and enzyme distribution in 3D-porous electrodes: a combined electrochemical and modelling study of a thermostable H_2/O_2 enzymatic fuel cell, Energy Environ. Sci. 10 (2017) 1966–1982.
[19] X. Xiao, H. Li, K. Zhang, P. Si, Examining the effects of self-assembled monolayers on nanoporous gold based amperometric glucose biosensors, Analyst 139 (2014) 488–494.
[20] X. Yan, C.U. Jansen, F. Diao, K. Qvortrup, D. Tanner, J. Ulstrup, X. Xiao, Surface-confined redox-active monolayers of a multifunctional anthraquinone derivative on nanoporous and single-crystal gold electrodes, Electrochem. Commun. 124 (2021) 106962.
[21] X. Yan, S. Ma, J. Tang, D. Tanner, J. Ulstrup, X. Xiao, J. Zhang, Direct electron transfer of fructose dehydrogenase immobilized on thiol-gold electrodes, Electrochim. Acta 392 (2021) 138946.
[22] S. Schindler, T. Bechtold, Mechanistic insights into the electrochemical oxidation of dopamine by cyclic voltammetry, J. Electroanal. Chem. 836 (2019) 94–101.
[23] X. Xiao, P.Ó. Conghaile, D. Leech, R. Ludwig, E. Magner, A symmetric supercapacitor/biofuel cell hybrid device based on enzyme-modified nanoporous gold: an autonomous pulse generator, Biosens. Bioelectron. 90 (2017) 96–102.
[24] S. Trasatti, O.A. Petrii, Real surface area measurements in electrochemistry, Pure Appl. Chem. 63 (1991) 711–734.
[25] G.T. Gnahore, T. Velasco-Torrijos, J. Colleran, The selective electrochemical detection of dopamine using a sulfated β-Cyclodextrin carbon paste electrode, Electrocatalysis 8 (2017) 459–471.
[26] X. Xiao, P.Ó. Conghaile, D. Leech, R. Ludwig, E. Magner, An oxygen-independent and membrane-less glucose Biobattery/Supercapacitor hybrid device, Biosens. Bioelectron. 98 (2017) 421–427.
[27] X. Xiao, K.Denis McGourty, E. Magner, Enzymatic biofuel cells for self-powered, controlled drug release, J. Am. Chem. Soc. 142 (2020) 11602–11609.
[28] X. Xiao, X. Yan, E. Magner, J. Ulstrup, Polymer coating for improved redox-polymer-mediated enzyme electrodes: a mini-review, Electrochem. Commun. 124 (2021) 106931.
[29] A. Ruff, Redox Polymers in Bioelectrochemistry: common Playgrounds and Novel Concepts, Curr. Opin. Electrochem. 5 (2017) 66–73.
[30] G.A. Mabbott, An introduction to cyclic voltammetry, J. Chem. Educ. 60 (1983) 697.
[31] J. Heinze, Cyclic Voltammetry—"Electrochemical Spectroscopy", Angew. Chem. Int. Ed. 23 (25) (1984) 831–847.
[32] R.R. Nazmutdinov, S.A. Shermokhamedov, T.T. Zinkicheva, J. Ulstrup, X. Xiao, Understanding molecular and electrochemical charge transfer: theory and computations, Chem. Soc. Rev. 52 (2023) 6230–6253.
[33] U.E. Majewska, K. Chmurski, K. Biesiada, A.R. Olszyna, R. Bilewicz, Dopamine Oxidation at Per(6-deoxy-6-thio)-α-Cyclodextrin Monolayer Modified Gold Electrodes, Electroanalysis 18 (2006) 1463–1470.
[34] M.D. Hawley, S.V. Tatawawadi, S. Piekarski, R.N. Adams, Electrochemical studies of the oxidation pathways of catecholamines, J. Am. Chem. Soc. 89 (1967) 447–450.
[35] H. Cao, Z. Zheng, P. Norby, X. Xiao, S. Mossin, Electrochemically induced phase transition in $V_3O_7 \cdot H_2O$ nanobelts/reduced graphene oxide composites for aqueous zinc-ion batteries, Small 17 (2021) 2100558.
[36] S. Li, Y. Yang, Z. Hu, S. Li, F. Ding, X. Xiao, P. Si, J. Ulstrup, Hetero-structured NiS_2/CoS_2 nanospheres embedded on N/S co-doped carbon nanocages with ultra-thin nanosheets for hybrid supercapacitors, Electrochim. Acta 424 (2022) 140604.
[37] E.Ö. Jónsson, K.S. Thygesen, J. Ulstrup, K.W. Jacobsen, Ab initio calculations of the electronic properties of polypyridine transition metal complexes and their adsorption on metal surfaces in the presence of solvent and counterions, J. Phys. Chem. B 115 (2011) 9410–9416.
[38] A. Heller, Electron-conducting redox hydrogels: design, characteristics and synthesis, Curr. Opin. Chem. Biol. 10 (2006) 664–672.
[39] T. Adachi, Y. Kaida, Y. Kitazumi, O. Shirai, K. Kano, Bioelectrocatalytic performance of D-fructose dehydrogenase, Bioelectrochem 129 (2019) 1–9.
[40] Y. Suzuki, F. Makino, T. Miyata, H. Tanaka, K. Namba, K. Kano, K. Sowa, Y. Kitazumi, O. Shirai, Essential insight of direct electron transfer-type bioelectrocatalysis by membrane-bound d-fructose dehydrogenase with structural bioelectrochemistry, ACS Catal 13 (2023) 13828–13837.
[41] I. Mazurenko, K. Monsalve, J. Rouhana, P. Parent, C. Laffon, A.L. Goff, S. Szunerits, R. Boukherroub, M.-T. Giudici-Orticoni, N. Mano, E. Lojou, How the intricate interactions between carbon nanotubes and two bilirubin oxidases control direct and mediated O2 reduction, ACS Appl. Mater. Interfaces 8 (2016) 23074–23085.